BRAIN RESEARCH 1109 (2006) 192–200

available at www.sciencedirect.com

ScienceDirect

www.elsevier.com/locate/brainres

BRAIN RESEARCH

Research Report

A new model of retinal photoreceptor cell degeneration induced by a chemical hypoxia-mimicking agent, cobalt chloride

Akira Hara[a,*], *Masayuki Niwa*[b,c], *Hitomi Aoki*[e], *Masako Kumada*[d], *Takahiro Kunisada*[e], *Takeru Oyama*[a], *Tetsuya Yamamoto*[d], *Osamu Kozawa*[b], *Hideki Mori*[a]

[a]*Department of Tumor Pathology, Gifu University Graduate School of Medicine, 1-1 Yanagido, Gifu 501-1194, Japan*
[b]*Department of Pharmacology, Gifu University School of Medicine, 1-1 Yanagido, Gifu 501-1194, Japan*
[c]*Medical Education Development Center, Gifu University School of Medicine, 1-1 Yanagido, Gifu 501-1194, Japan*
[d]*Department of Ophthalmology, Gifu University School of Medicine, 1-1 Yanagido, Gifu 501-1194, Japan*
[e]*Department of Tissue and Organ Development, Gifu University Graduate School of Medicine, 1-1 Yanagido, Gifu 501-1194, Japan*

ARTICLE INFO

Article history:
Accepted 14 June 2006
Available online 25 July 2006

Keywords:
Retina
Photoreceptor cell
Degeneration
Cobalt chloride
Hypoxia

ABSTRACT

Retinal photoreceptor cell degeneration was induced by cobalt chloride, a chemical hypoxia-mimicking agent in rodents. Time course and dose–response of photoreceptor cell degeneration in mouse retina after intravitreal injection of cobalt chloride were examined by conventional histological analysis by hematoxylin and eosin staining and in situ terminal dUTP-biotin nick end labeling of DNA fragments (TUNEL) method with the use of paraffin-embedded sections. The dose–response of photoreceptor cell degeneration in rat retina was also examined. Photoreceptor cells progressively degenerated with time and under dose–response relationship. The suitable dose of cobalt chloride for the selective photoreceptor cell degeneration in mice is 10–12 nmol intravitreal injection at the volume of 2 μl. The retinal morphology of the mice 2 weeks after the 10–12 nmol intravitreal injection was similar to that of retinal degeneration in the mutant *rd* mouse. Retinal damage of total retinal layers was induced by an excessive dose of cobalt chloride. The progression of retinal damage after cobalt chloride injection, measured morphologically, was completed at 1 week. However, nuclear DNA fragmentation, mainly detected at outer nuclear layer by TUNEL, peaked at 48 h after 12 nmol cobalt chloride injection. Thus, the selective photoreceptor cell degeneration induced by cobalt chloride follows DNA fragmentation at outer nuclear layer. The photoreceptor cell degeneration is established optionally by cobalt chloride without use of the retinal degeneration mutant animals. Thus, we have described the development of a new model of retinal photoreceptor cell degeneration induced by a chemical hypoxia-mimicking agent.

* *Corresponding author.* Fax: +81 58 230 6226.
E-mail address: ahara@cc.gifu-u.ac.jp (A. Hara).

0006-8993/$ – see front matter © 2006 Elsevier B.V. All rights reserved.
doi:10.1016/j.brainres.2006.06.037

1. Introduction

Retinal degenerative diseases, either acquired or inherited, are a major cause of visual impairment and blindness in humans. Most retinal degeneration caused by genetic mutations affect the retinal pigment epithelium and sensory retina. For example, retinitis pigmentosa (RP), which is characterized by a progressive loss of photoreceptors through mechanisms not yet fully understood, is a leading cause of blindness and visual disability in younger people (Berson, 1993). Mutations in a number of different genes (such as rhodopsin, the beta subunit of cGMP phosphodiesterase and peripherin) have been identified as the primary genetic lesion in different forms of human retinitis pigmentosa (Kennan et al., 2005). Age-related macular degeneration (AMD), which is a diffuse condition involving the retinal pigment epithelium, is also recognized as a complex genetic disorder in which one or more genes contribute to an individual's susceptibility for developing the condition (Green, 1999; Zack et al., 1999). The condition of these diseases is currently incurable, and there are still many obstacles that need to be overcome before treatments including gene therapy or cell replacement therapy can be applied to humans (Delyfer et al., 2004; Yu and Cringle, 2005).

Many animal models of retinal degeneration are available and have led to a better understanding of the disease and to the development of possible therapeutic strategies. A well-established animal model of retinal degeneration, rd mouse, possesses a mutation of the rod-specific phosphodiesterase and leads to the rapid and massive death of rod photoreceptors in the first few weeks of postnatal life (Bowes et al., 1990) and then leads to blindness with subsequent cone degeneration in less than 2 months (Jimenez et al., 1996). Animal models with spontaneous retinal degeneration have been used for many years to study disease progression and pathology. Many of these animal models have come from screening mice from genetically independent mouse strains (Chang et al., 1993; Hawes et al., 2000).

The involvement of the genetic aspects of retinal degeneration is well established (Berson, 1993; Chang et al., 1993; Hawes et al., 2000), but there is much less known about the environmental and metabolic aspects of the degenerative process. The loss of photoreceptors themselves will inevitably induce metabolic changes in the remaining retina. In particular, a role for the local oxygen environment within the retina has been proposed (Yu and Cringle, 2005). In animal models of photoreceptor degeneration, manipulation of environmental oxygen levels has been reported to be able to modulate the rate of photoreceptor degeneration (Maslim et al., 1997; Valter et al., 1998).

Cobalt chloride has been widely used as a hypoxia-mimicking agent in both in vivo (Badr et al., 1999) and in vitro studies (Wang and Semenza, 1993). Many reports have shown that both cobalt and hypoxia regulate a similar group of genes on a global gene expression level (Ji et al., in press; Lee et al., 2001; Vengellur et al., 2003). Cobalt is essential for human health because of its critical role in the synthesis of vitamin B12 (Roessner et al., 2001), however, excess exposure of cobalt can lead to tissue and cellular toxicity. In the present study, a new model of photoreceptor cell degeneration induced by intravitreal injection of cobalt chloride is presented.

2. Results

2.1. *Histologic evaluation of the retinal degeneration*

Photoreceptor cells progressively degenerated with time (Fig. 2) and under dose–response relationship (Figs. 1 and 3). Various retinal lesions were caused by intravitreal injection of cobalt chloride (Figs. 1, 2 and 3). To determine a suitable dose of cobalt chloride for the selective photoreceptor cell degeneration, the morphological changes characterized by hematoxylin and eosin (HE) staining in each retina were scored semi-quantitatively by microscopic examination as follows: negative, 0; minimal morphological changes of the

Fig. 1 – Representative microphotographs of histological examination by hematoxylin and eosin staining in mouse retina 2 weeks after treatment of each dose of cobalt chloride. (A) 1, (B) 2, (C) 5, (D) 10 and (E) 20 nmol cobalt chloride in 2 μl of distilled water was injected intravitreally. As described in Results, the cobalt-chloride-induced morphological changes in each retina were scored semi-quantitatively. In panel A, no morphological change was recognized, thus scored as 0. The morphological changes of retinal cell degeneration in panels B, C, D and E were scored 1, 2, 3 and 4, respectively. GCL, ganglion cell layer; INL, inner nuclear layer; ONL, outer nuclear layer. Scale bar in panel A, 50 μm.

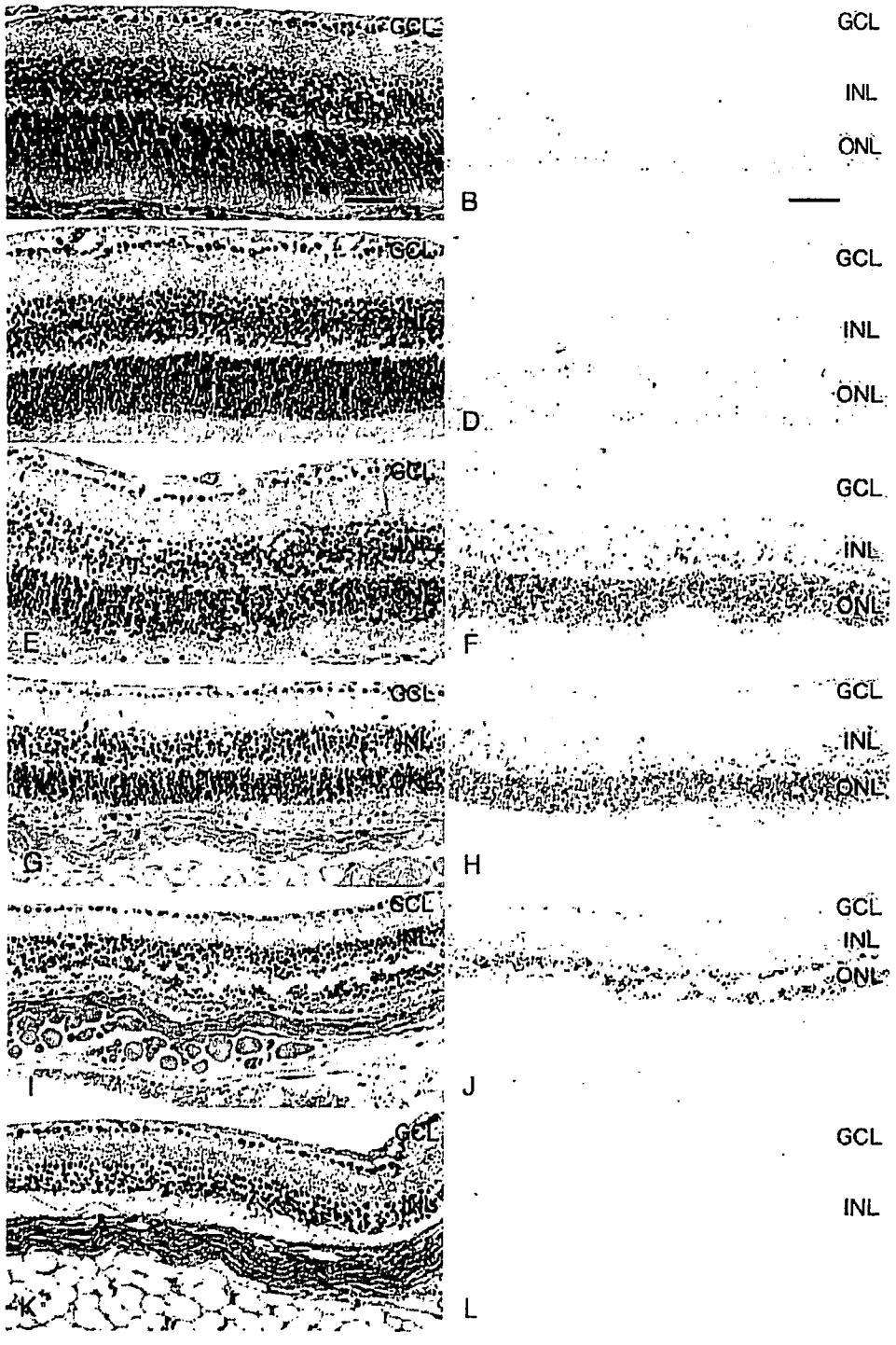

Fig. 2 – Time course analysis for mouse retina detected by hematoxylin and eosin staining (A, C, E, G, I, K) and TUNEL staining (B, D, F, H, J, L) at 12 (A, B), 24 (C, D), 48 (E, F) and 96 h (G, H) and 1 (I, J) and 2 weeks (K, L) after intravitreal cobalt chloride injection at the dose of 12 nmol. There is no morphological damage 12 and 24 h after intravitreal injection (A, C). No TUNEL-positive apoptotic cells are seen at 12 h (B), however, a few TUNEL-positive cells are seen at 24 h (D). TUNEL-positive cells peaked at 48 h after injection (F). Only small numbers of nuclei in ONL are seen at 1 week after the injection (I, J), and the ONL disappeared at 2 weeks (K, L). GCL, ganglion cell layer; INL, inner nuclear layer; ONL, outer nuclear layer. Scale bar in panels A and B, 50 μm.

outer nuclear layer (ONL) in retina, 1; atrophy of ONL, 2; disappearance of ONL, 3; and damage of total retinal layers, 4. Most severe lesion was evaluated and scored in each retina. The mean score of each group of cobalt-chloride-treated retina was defined as retinal damage index (RDI). Furthermore, photoreceptor damage rate (PDR) was defined as the ratio of

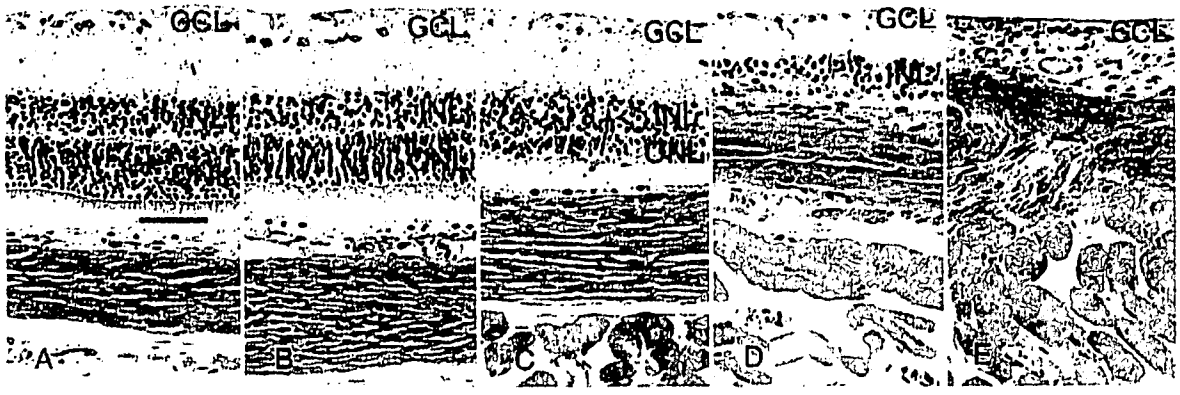

Fig. 3 – Representative microphotographs of histological examination by hematoxylin and eosin staining in rat retina 2 weeks after treatment of each dose of cobalt chloride. (A) 5, (B) 15, (C) 50, (D) 150 and (E) 500 nmol cobalt chloride in 5 μl of distilled water was injected intravitreally. As described in Results, the cobalt-chloride-induced morphological changes in each retina were scored semi-quantitatively. In panel A, no morphological change was recognized, thus scored 0. The morphological changes of retinal cell degeneration in panels B, C, D and E were scored 1, 2, 3 and 4, respectively. GCL, ganglion cell layer; INL, inner nuclear layer; ONL, outer nuclear layer. Scale bar in panel A, 50 μm.

the retinal area showing selective photoreceptor cell degeneration to all the retinal area. Total retina damage rate (TDR) was defined as the ratio of the retinal area showing the damage of total retinal layer to all the retinal area. RDI was used for the time course analysis for mouse retina, and dose–response analyses for mouse and rat retina. PDR and TDR rate was used for the dose–response analyses for mouse and rat retina.

2.2. *Apoptotic evaluation of the retinal degeneration*

The nuclear DNA fragmentation recognized as brown stain in ONL by in situ terminal dUTP-biotin nick end labeling of DNA fragments (TUNEL) method (Fig. 2) was scored semi-quantitatively by microscopic examination as follows: negative, 0; less than 50% of apoptotic cells in ONL, 1; more than 50% of apoptotic cells in ONL, 2; and apoptotic cells recognized as total retinal damage, 3. Most severe apoptotic lesion was evaluated and scored in each retina. The mean score of each group was defined as retinal apoptotic index (RAI). RAI was used for the time course analysis for mouse retina. In the mouse retina showing selective photoreceptor cell degeneration, TUNEL-positive cells were detected exclusively in the ONL. At 48 h after the injection of 12 nmol cobalt chloride, the RAI reached a peak.

2.3. *Dose–response analysis for mouse retina*

Dose–response increase of RDI in mouse retina was shown by intravitreal injection of cobalt chloride (Fig. 4A). PDR gradually increased dose-dependently and peaked at 10 nmol treatment. At 20 nmol treatment, PDR decreased and TDR increased (Fig. 4B). This means that suitable concentration for the induction of selective photoreceptor cell degeneration is 10 nmol cobalt chloride in mouse retina. Under these conditions, the photoreceptor outer segments were totally absent and the ONL could not be identified. In contrast, ganglion cell layer and inner nuclear layer were well preserved (Fig. 1D). This retinal morphology resembles the retinal degeneration that occurs in the mutant *rd* mouse.

2.4. *Time course analysis for mouse retina*

The results of the time course analysis for mouse retina at the dose of 12 nmol and 18 nmol of cobalt chloride are presented in Figs. 5A and B, respectively. At the dose of 12 nmol cobalt chloride, there was no retinal damage at 12 and 24 h after intravitreal injection. RDI increased from 48 h after injection and the retinal damage was complete at 1 week after injection. At the dose of 18 nmol cobalt chloride, RDI increased from 24 h after injection and the retinal damage was complete at 1 week after injection. RDI at 2 and 4 weeks were stable at both doses of cobalt chloride. This means the damaged lesions were irreversible. More severe lesions were seen at 18 nmol compared with that of 12 nmol cobalt chloride. The TUNEL-positive cells preceded morphological cell damage in ONL and RAI peaked at 48 h after the drug injection (Figs. 5A and B).

2.5. *Dose–response analysis for rat retina*

Dose–response increase of RDI in rat retina was also shown in the same manner of mouse by intravitreal injection of cobalt chloride (Fig. 6A). PDR gradually increased dose-dependently and peaked at 50 nmol cobalt chloride (Fig. 6B). Severe retinal damages occurred at 150 and 500 nmol (Fig. 6B). At the concentration for the induction of selective photoreceptor cell degeneration, the photoreceptor outer segments were totally absent and the ONL could not be identified (Fig. 3D). In contrast, ganglion cell layer and inner nuclear layer were well preserved.

3. Discussion

Although it is well known that the retina is one of the most metabolically active tissues in the body and oxygen is known to be the most supply-limited metabolite in the retina (Trick and Berkowitz, 2005), possible roles of the metabolic

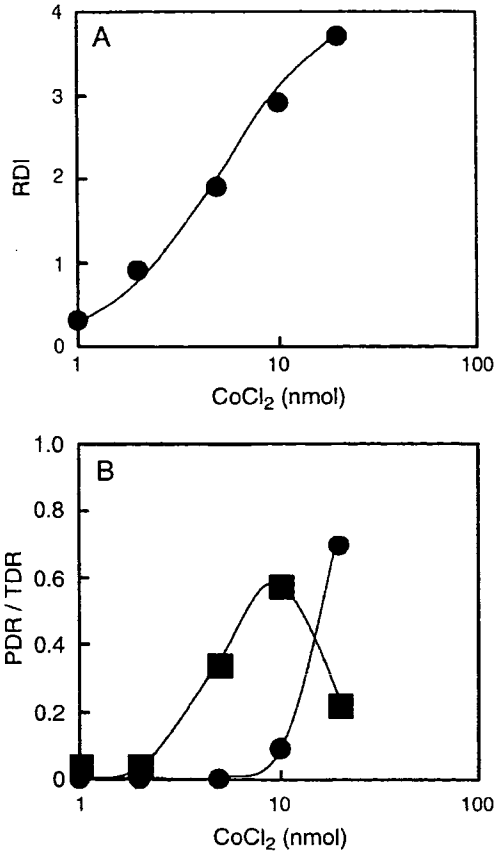

Fig. 4 – Dose–response analysis of mouse retinal damage 2 weeks after intravitreal injection at each dose of cobalt chloride. As described in Results, the cobalt-chloride-induced morphological changes in each retina was scored semi-quantitatively. The mean score of each group of cobalt-chloride-treated retina was defined as RDI. PDR was defined as the ratio of the retinal area showing selective photoreceptor cell degeneration to all the retinal area. TDR was defined as the ratio of the retinal area showing the damage of total retinal layer to all the retinal area. RDI (●) is plotted in panel A, and PDR (■) and TDR (●) are plotted in panel B. RDI, retinal damage index; PDR, photoreceptor damage rate; TDR, total retina damage rate.

microenvironment of the retina in the retinal degenerative process have not been clarified yet (Yu and Cringle, 2005). Because a continuous supply of oxygen is necessary to maintain retinal function, oxygen deprivation results in significant and permanent retinal dysfunction. In animal mutant models of photoreceptor degeneration, manipulation of environmental oxygen levels has been reported to be able to modulate the rate of photoreceptor degeneration (Maslim et al., 1997; Valter et al., 1998). Metabolic changes within the retina in the early phase of degenerative process may also contribute to the further progression of photoreceptor cell loss (Yu and Cringle, 2005; Yu et al., 2005).

In the present study, retinal photoreceptor cell degeneration was induced by cobalt chloride, which provides chemically induced hypoxia-mimicking conditions, both in mice and in rats. Photoreceptor cells progressively degenerated with time and dose dependency. The ONL-specific photoreceptor cell degeneration was induced by intravitreal injection of cobalt chloride, at 10–12 nmol in mice and 50 nmol in rats. The retinal morphology of the mice observed 2 weeks after the cobalt chloride injection resembles retinal degeneration seen in the mutant *rd* mouse. The photoreceptor cell degeneration can be produced by cobalt chloride without use of the retinal degeneration mutant animals.

Cobalt chloride has been widely used as a hypoxia-mimicking agent in both in vivo (Badr et al., 1999) and in vitro studies (Wang and Semenza, 1993).

The hypoxia-responsive pathway is specifically stimulated by exposure to cobalt chloride, which acts in the presence of oxygen without inhibition of oxidative phosphorylation (Badr et al., 1999). Cobalt chloride is a bioactive chemical. For example, it plays a critical role in the synthesis of vitamin B12. And it acts as a hypoxia-mimicking agent leading to enhanced expression of a set of hypoxia-responsive genes (Vengellur and LaPres, 2004; Vengellur et al., 2003). Many reports have shown that both cobalt and hypoxia regulate a similar group of genes on a global gene expression level (Ji et

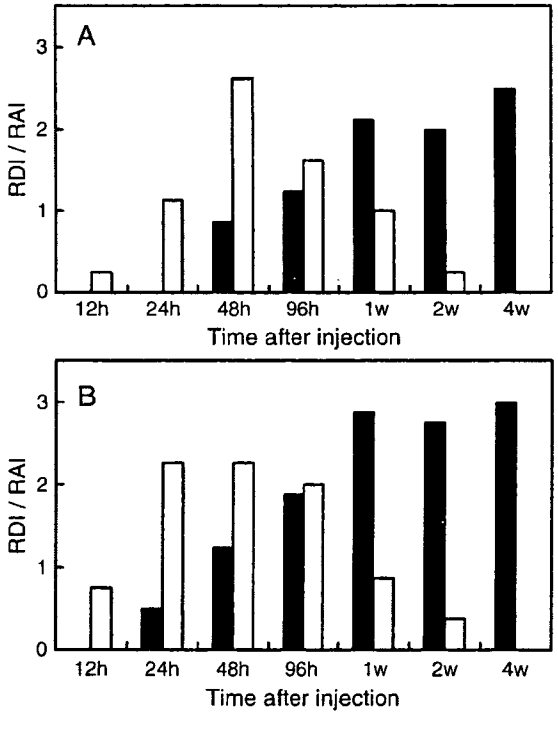

Fig. 5 – Time course of retinal damage detected by hematoxylin and eosin (HE) staining and TUNEL method at the dose of 12 nmol (A) and 18 nmol of cobalt chloride (B). As described in Results, the cobalt-chloride-induced morphological changes in each retina were scored semi-quantitatively and the TUNEL-positive apoptotic cells in ONL were also scored semi-quantitatively. The mean score of HE staining in each group of cobalt-chloride-treated retina was defined as RDI. The mean TUNEL score of each group was defined as RAI. RDI, retinal damage index; RAI, retinal apoptotic index. ■, RDI; □, RAI.

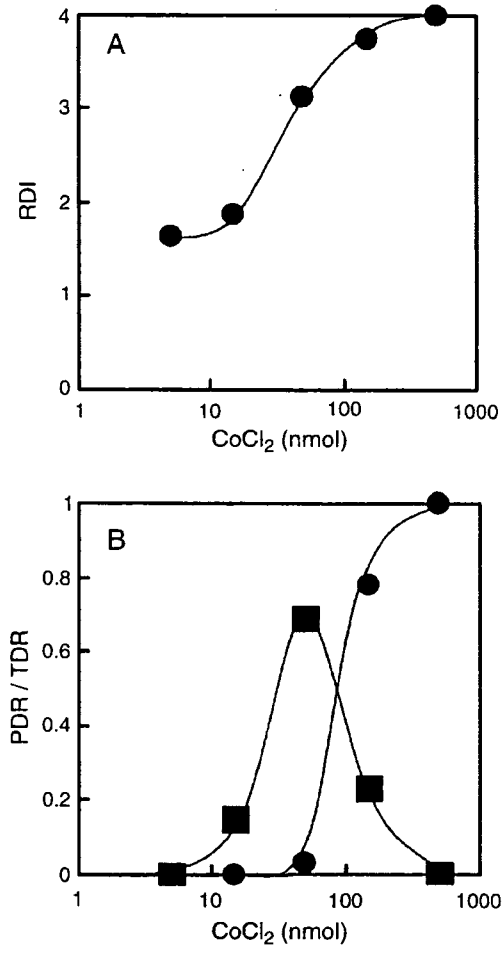

Fig. 6 – Dose–response analysis of rat retinal damage 2 weeks after intravitreal injection at each dose of cobalt chloride. As described in Results, the cobalt-chloride-induced morphological changes in each retina were scored semi-quantitatively. RDI (●) is plotted in panel A, and PDR (■) and TDR (●) are plotted in panel B. RDI, retinal damage index; PDR, photoreceptor damage rate; TDR, total retina damage rate.

al., in press; Lee et al., 2001; Vengellur et al., 2003). In rat cerebrum and retina, exposure to cobalt chloride, presumably acting through the hypoxia-signaling pathway including hypoxia-inducible factors, results in enhanced expression of major glucose transporter associated proteins, without increasing the capillary density (Badr et al., 1999). Furthermore, many reports demonstrated that cobalt chloride could induce apoptosis in many different kinds of cells. For examples, cobalt chloride was shown to induce apoptosis in rat C6 glioma cells (Yang et al., 2004), human alveolar macrophages (Araya et al., 2002), neuronal PC12 cells (Zou et al., 2001) and HeLa human cervical cancer cells (Kim et al., 2003). Our results also demonstrated that cobalt chloride is an apotopsis-inducing agent before retinal degeneration, which acts specifically in the photoreceptor cells.

Although an excessive dose of cobalt chloride damaged total retinal layers at an appropriate dose, cobalt chloride induced the selective photoreceptor cell degeneration with the well-preserved inner retina in both mice and rats. Oxygen supply to the retina is derived from two separate vascular systems. The choroid provides oxygen to the outer retina, while the retinal circulation provides the oxygen requirements of the inner retina. The retinal circulation is relatively sparse (presumably to allow passage of light to the photoreceptors), however, the choroid is highly vascularized. The extremely high oxygen consumption occurs in the inner segments of the photoreceptors, which are supplied from the vascular-rich choroid (Yu and Cringle, 2005). Thus, photoreceptor cells are considered more vulnerable than any other retinal cells to hypoxia-mimicking conditions induced by intravitreal injection of cobalt chloride. Interestingly, the adult rat retina is vulnerable to both hypoxia (air with the concentration of oxygen at 10%) and hyperoxia (45%, 65%, 70% and 75%) examined under real oxygen condition (Wellard et al., 2005). The vulnerability under the conditions is also specific to photoreceptors, and other retinal neurons have appeared resistant to the oxygen levels (Wellard et al., 2005).

The retina is an essential neural compartment and is used experimentally for understanding the development of the central nervous system (Hara et al., 2004b; Jones and Marc, 2005). Thus, it is hoped that the results from animal models of hypoxia-related retinal degeneration could provide relevant information for improving strategies for therapeutic intervention in ischemic insults of the human central nervous system. A number of reviews deal with the genetic aspects of retinal degeneration (Berson, 1993; Dryja and Berson, 1995), but there is much less known about the environmental and metabolic aspects, especially oxygen environment in the retinal degenerative process. Hyperoxia has been used to treat retinal degeneration clinically. Significant improvements have been reported in the electrophysiological responses in the treatment of retinitis pigmentosa patients with hyperbaric oxygen therapy (Vingolo et al., 1998).

In inner retina, intravitreal injection of *N*-methyl-D-aspartate (NMDA), a glutamate receptor agonist, is a good model for in vivo neuronal degeneration since glutamate-induced excitotoxicity is associated with a selective loss of retinal neurons after retinal ischemia and possibly in glaucoma (Kumada et al., 2004, 2005). Glutamate, or related excitatory amino acids, is thought to mediate excitatory synaptic transmission acting through activation of glutamate receptors (Sucher et al., 1997). Since glutamate is probably the excitatory transmitter used by retinal ganglion cells, the intravitreal NMDA injection model seems to be based on the intrinsic system of synaptic transmission.

In the present study, intravitreal injection of cobalt chloride, which provides chemically induced hypoxia-mimicking conditions, is also considered a good model for in vivo retinal photoreceptor degeneration because of the vulnerability of photoreceptor cells to oxygen environment in the degenerative process. On the other hand, the retinal morphology observed 2 weeks after the cobalt chloride injection resembles the retinal degeneration that occurs in the mutant *rd* mouse. This suggests that the photoreceptor cell degenerations in both the genetic aspects and the

metabolic aspects are based on a similar cytological process. In fact, apoptosis is the final common pathway and precedes the morphological changes of photoreceptor cells in many cases of retinal degeneration.

In addition to the model for the vulnerability of photoreceptor cells to oxygen environment in the degenerative process, cobalt-chloride-treated animal can be used as a recipient for tissue regeneration model. Usually, rd mouse is utilized as a recipient animal to assess the capacity for the grafted neural progenitor cells (Lu et al., 2002) or embryonic stem cells (Meyer et al., 2004). Our model can be also used as a recipient animal for tissue regeneration without use of the animals possessing gene mutations. Further studies are necessary to clarify the roles of cobalt chloride in expression of hypoxia-responsive genes in retina and the applications of cobalt-chloride-treated retina in the research of tissue regeneration.

4. Experimental procedures

4.1. Animals

Male ddY mice (6–7 weeks) were purchased from a local supplier (Chubukagakusizai, Co., Japan) and maintained under 12 h light:12 h dark cyclic lighting conditions. Male Wistar rats (6–7 weeks) were also purchased from the same supplier and maintained under the same conditions.

4.2. Intravitreal injection to mice

The method to inject cobalt chloride solution was performed with some modifications to the method by Timmers et al. (2001). Mice were anesthetized with intraperitoneal injection of 50 mg/kg sodium pentobarbital (Nembutal, Dainippon Pharmaceutical. Co. Ltd., Japan). Animals were placed in the pronate position under the SN MD-II operation microscope (Nagashima Medical Instruments Co., LTD, Japan). Pupils were then dilated with one drop of 0.5% phenylephrine hydrochloride–0.5% tropicamide solution (Mydrin P, Santen Pharmaceutical, Japan). Topical anesthetics were performed with one drop of 0.4% oxybuprocaine (Benoxil, Santen Pharmaceutical, Japan). Mouse fundus was visualized with a drop of 1.5% hydroxycellulose (SCOPISOL15, Senju Pharmaceutical, Japan) to the eye. The cornea was carefully punctured nasally approximately 0.5 mm medial to the dilated papillary margin using a 30-gauge hypodermic needle (Becton Dickinson and Company, NJ). The needle was advanced through the cornea into the anterior chamber and then injected 2 μl of hyaluronate sodium (Healon, Pfizer Pharmaceutical, NY or VISCORT, Alcon, TX) along the inside of the cornea. Then, 33-gauge blunt needle (Hamilton Company, NV) was inserted through the corneal puncture and advanced into anterior chamber, avoiding trauma to the iris and lens. Subsequently, needle shaft was aimed to posterior chamber, lateral from iris and medial toward lens. The lens was displaced medially as the needle was advanced to the surface of retina through the vitreous cavity. When the tip of the needle reached to the desired injection location, 2 μl of cobalt chloride solution was injected slowly and keep the position approximately 30 s. The viscosity of the hyaluronate sodium placed in anterior chamber avoids a small amount of reflux of injected material through the corneal wound.

4.3. Intravitreal injection to rats

The method to inject cobalt chloride solution was performed with the same method as mice. Rats were anesthetized and placed in the pronate position under the SN MD-II operation microscope. Pupils were dilated with one drop of 0.5% phenylephrine hydrochloride–0.5% tropicamide solution, and topical anesthetics were performed with one drop of 0.4% oxybuprocaine. Rat fundus was visualized with a drop of 1.5% hydroxycellulose to the eye. The cornea was punctured nasally approximately 0.7 mm medial to the dilated papillary margin using a 30-gauge hypodermic needle. The needle was advanced through the cornea into the anterior chamber and then injected 5 μl of hyaluronate sodium along the inside of the cornea. Then, 33-gauge blunt needle was inserted through the corneal puncture. When the tip of the needle reached to the desired injection location, 5 μl of cobalt chloride solution was injected slowly and keep the position approximately 30 s in the same manner as mice.

4.4. Dose–response analysis for mouse retina

Five doses of cobalt chloride solution, 1, 2, 5, 10 and 20 nmol in 2 μl of distilled water, have been used for the dose–response study. The whole eyes were extracted at 2 weeks after intravitreal injection. Ten eyes per group were used for the experiment.

4.5. Time course analysis for mouse retina

The whole eyes were extracted at 0, 12, 48 and 96 h and 1, 2 and 4 weeks after intravitreal cobalt chloride injection. Two doses (12 nmol and 18 nmol) of cobalt chloride solution have been used for this study. Eight eyes per group were used for the experiment.

4.6. Dose–response analysis for rat retina

Five doses of cobalt chloride solution, 5, 15, 50, 150 and 500 nmol in 5 μl of distilled water, have been used for the dose–response study. The whole eyes were extracted at 2 weeks after intravitreal injection. Eight eyes per group were used for the experiment.

4.7. Histologic processing

The mice and rats were killed with an overdose of pentobarbital sodium. The specimens were fixed overnight in 10% phosphate-buffered formalin by setting on a mixing machine (MildMixer PR-36; TAITEC, Tokyo, Japan) and then embedded in paraffin. Two sequential sections were cut as 3 μm along vertical meridian through the optic nerve, placed on poly-L-lysine-coated microscopic slides and then used for HE staining and TUNEL method.

4.8. *TUNEL method*

TUNEL method was performed as described previously (Hara et al., 2004a; Kumada et al., 2005). After incubation with 20 mg/ml proteinase K (Sigma), the serial sections used for HE staining were immersed in TDT buffer (30 mM Trizma base, pH 7.2, 140 mM sodium cacodylate, 1 mM cobalt chloride). TDT (Boehringer Mannheim GmbH, Mannheim, Germany) and biotinylated dUTP (Boehringer Mannheim GmbH, Mannheim, Germany) were diluted in TDT buffer at a concentration of 0.15 e.u./ml and 0.8 nmol/ml, respectively. The solution was placed on the sections and then incubated at 37 °C for 60 min. The sections were covered with streptavidin peroxidase (DAKO, Carpinteria, USA) and stained with 3,3′-diaminobenzidine (DAB) as a substrate for the peroxidase. Finally, counterstaining was done using Mayer's hematoxylin.

REFERENCES

Araya, J., Maruyama, M., Inoue, A., Fujita, T., Kawahara, J., Sassa, K., Hayashi, R., Kawagishi, Y., Yamashita, N., Sugiyama, E., Kobayashi, M., 2002. Inhibition of proteasome activity is involved in cobalt-induced apoptosis of human alveolar macrophages. Am. J. Physiol.: Lung Cell. Mol. Physiol. 283, L849–L858.

Badr, G.A., Zhang, J.Z., Tang, J., Kern, T.S., Ismail-Beigi, F., 1999. Glut1 and glut3 expression, but not capillary density, is increased by cobalt chloride in rat cerebrum and retina. Brain Res. Mol. Brain Res. 64, 24–33.

Berson, E.L., 1993. Retinitis pigmentosa. The Friedenwald Lecture. Invest. Ophthalmol. Visual Sci. 34, 1659–1676.

Bowes, C., Li, T., Danciger, M., Baxter, L.C., Applebury, M.L., Farber, D.B., 1990. Retinal degeneration in the rd mouse is caused by a defect in the beta subunit of rod cGMP-phosphodiesterase. Nature 347, 677–680.

Chang, B., Heckenlively, J.R., Hawes, N.L., Roderick, T.H., 1993. New mouse primary retinal degeneration (rd-3). Genomics 16, 45–49.

Delyfer, M.N., Leveillard, T., Mohand-Said, S., Hicks, D., Picaud, S., Sahel, J.A., 2004. Inherited retinal degenerations: therapeutic prospects. Biol. Cell 96, 261–269.

Dryja, T.P., Berson, E.L., 1995. Retinitis pigmentosa and allied diseases. Implications of genetic heterogeneity. Invest. Ophthalmol. Visual Sci. 36, 1197–1200.

Green, W.R., 1999. Histopathology of age-related macular degeneration. Mol. Vision 5, 27.

Hara, A., Niwa, M., Kumada, M., Kitaori, N., Yamamoto, T., Kozawa, O., Mori, H., 2004a. Fragmented DNA transport in dendrites of retinal neurons during apoptotic cell death. Brain Res. 1007, 183–187.

Hara, A., Niwa, M., Kunisada, T., Yoshimura, N., Katayama, M., Kozawa, O., Mori, H., 2004b. Embryonic stem cells are capable of generating a neuronal network in the adult mouse retina. Brain Res. 999, 216–221.

Hawes, N.L., Chang, B., Hageman, G.S., Nusinowitz, S., Nishina, P.M., Schneider, B.S., Smith, R.S., Roderick, T.H., Davisson, M.T., Heckenlively, J.R., 2000. Retinal degeneration 6 (rd6): a new mouse model for human retinitis punctata albescens. Invest. Ophthalmol. Visual Sci. 41, 3149–3157.

Ji, Z., Yang, G., Shahzidi, S., Tkacz-Stachowska, K., Suo, Z., Nesland, J.M., Peng, Q., in press. Induction of hypoxia-inducible factor-1alpha overexpression by cobalt chloride enhances cellular resistance to photodynamic therapy. Cancer Lett.

Jimenez, A.J., Garcia-Fernandez, J.M., Gonzalez, B., Foster, R.G., 1996. The spatio-temporal pattern of photoreceptor degeneration in the aged rd/rd mouse retina. Cell Tissue Res. 284, 193–202.

Jones, B.W., Marc, R.E., 2005. Retinal remodeling during retinal degeneration. Exp. Eye Res. 81, 123–137.

Kennan, A., Aherne, A., Humphries, P., 2005. Light in retinitis pigmentosa. Trends Genet. 21, 103–110.

Kim, H.J., Yang, S.J., Kim, Y.S., Kim, T.U., 2003. Cobalt chloride-induced apoptosis and extracellular signal-regulated protein kinase activation in human cervical cancer HeLa cells. J. Biochem. Mol. Biol. 36, 468–474.

Kumada, M., Niwa, M., Wang, X., Matsuno, H., Hara, A., Mori, H., Matsuo, O., Yamamoto, T., Kozawa, O., 2004. Endogenous tissue type plasminogen activator facilitates NMDA-induced retinal damage. Toxicol. Appl. Pharmacol. 200, 48–53.

Kumada, M., Niwa, M., Hara, A., Matsuno, H., Mori, H., Ueshima, S., Matsuo, O., Yamamoto, T., Kozawa, O., 2005. Tissue type plasminogen activator facilitates NMDA-receptor-mediated retinal apoptosis through an independent fibrinolytic cascade. Invest. Ophthalmol. Visual Sci. 46, 1504–1507.

Lee, S.G., Lee, H., Rho, H.M., 2001. Transcriptional repression of the human p53 gene by cobalt chloride mimicking hypoxia. FEBS Lett. 507, 259–263.

Lu, B., Kwan, T., Kurimoto, Y., Shatos, M., Lund, R.D., Young, M.J., 2002. Transplantation of EGF-responsive neurospheres from GFP transgenic mice into the eyes of rd mice. Brain Res. 943, 292–300.

Maslim, J., Valter, K., Egensperger, R., Hollander, H., Stone, J., 1997. Tissue oxygen during a critical developmental period controls the death and survival of photoreceptors. Invest. Ophthalmol. Visual Sci. 38, 1667–1677.

Meyer, J.S., Katz, M.L., Maruniak, J.A., Kirk, M.D., 2004. Neural differentiation of mouse embryonic stem cells in vitro and after transplantation into eyes of mutant mice with rapid retinal degeneration. Brain Res. 1014, 131–144.

Roessner, C.A., Santander, P.J., Scott, A.I., 2001. Multiple biosynthetic pathways for vitamin B12: variations on a central theme. Vitam. Horm. 61, 267–297.

Sucher, N.J., Lipton, S.A., Dreyer, E.B., 1997. Molecular basis of glutamate toxicity in retinal ganglion cells. Vision Res. 37, 3483–3493.

Timmers, A.M., Zhang, H., Squitieri, A., Gonzalez-Pola, C., 2001. Subretinal injections in rodent eyes: effects on electrophysiology and histology of rat retina. Mol. Vision 7, 131–137.

Trick, G.L., Berkowitz, B.A., 2005. Retinal oxygenation response and retinopathy. Prog. Retinal Eye Res. 24, 259–274.

Valter, K., Maslim, J., Bowers, F., Stone, J., 1998. Photoreceptor dystrophy in the RCS rat: roles of oxygen, debris, and bFGF. Invest. Ophthalmol. Visual Sci. 39, 2427–2442.

Vengellur, A., LaPres, J.J., 2004. The role of hypoxia inducible factor 1alpha in cobalt chloride induced cell death in mouse embryonic fibroblasts. Toxicol. Sci. 82, 638–646.

Vengellur, A., Woods, B.G., Ryan, H.E., Johnson, R.S., LaPres, J.J., 2003. Gene expression profiling of the hypoxia signaling pathway in hypoxia-inducible factor 1alpha null mouse embryonic fibroblasts. Gene Expression 11, 181–197.

Vingolo, E.M., Pelaia, P., Forte, R., Rocco, M., Giusti, C., Rispoli, E., 1998. Does hyperbaric oxygen (HBO) delivery rescue retinal photoreceptors in retinitis pigmentosa? Doc. Ophthalmol. 97, 33–39.

Wang, G.L., Semenza, G.L., 1993. Desferrioxamine induces erythropoietin gene expression and hypoxia-inducible factor 1 DNA-binding activity: implications for models of hypoxia signal transduction. Blood 82, 3610–3615.

Wellard, J., Lee, D., Valter, K., Stone, J., 2005. Photoreceptors in the rat retina are specifically vulnerable to both hypoxia and hyperoxia. Vis. Neurosci. 22, 501–507.

Yang, S.J., Pyen, J., Lee, I., Lee, H., Kim, Y., Kim, T., 2004. Cobalt

chloride-induced apoptosis and extracellular signal-regulated protein kinase 1/2 activation in rat C6 glioma cells. J. Biochem. Mol. Biol. 37, 480–486.
Yu, D.Y., Cringle, S.J., 2005. Retinal degeneration and local oxygen metabolism. Exp. Eye Res. 80, 745–751.
Yu, D.Y., Cringle, S.J., Su, E.N., 2005. Intraretinal oxygen distribution in the monkey retina and the response to systemic hyperoxia. Invest. Ophthalmol. Visual Sci. 46, 4728–4733.
Zack, D.J., Dean, M., Molday, R.S., Nathans, J., Redmond, T.M., Stone, E.M., Swaroop, A., Valle, D., Weber, B.H., 1999. What can we learn about age-related macular degeneration from other retinal diseases? Mol. Vision 5, 30.
Zou, W., Yan, M., Xu, W., Huo, H., Sun, L., Zheng, Z., Liu, X., 2001. Cobalt chloride induces PC12 cells apoptosis through reactive oxygen species and accompanied by AP-1 activation. J. Neurosci. Res. 64, 646–653.

Proceedings of the 29th Annual International
Conference of the IEEE EMBS
Cité Internationale, Lyon, France
August 23-26, 2007.

Three-Dimensional Reconstruction of Optic Nerve Head from Stereo Fundus Images and Its Quantitative Estimation

Toshiaki Nakagawa, Yoshinori Hayashi, Yuji Hatanaka, Akira Aoyama, Takeshi Hara, Akihiro Fujita, Masakatsu Kakogawa, Hiroshi Fujita, and Tetsuya Yamamoto

Abstract— **It is important for diagnosis of glaucoma to grasp 3-D structure of an optic nerve head (ONH). The quantitative 3-D reconstruction of the ONH is required for the diagnosis. We propose a technique to obtain the depth value from stereo image pair of a retinal fundus for the 3-D reconstruction of the ONH. Our technique mainly consists of four steps: (1) cutout of the ONH region from the fundus images, (2) registration of the stereo pair, (3) disparity detection, and (4) depth calculation. For quantitative estimation of the depth value measured by using this method, the depth value was compared with the measurement results determined from the Heidelberg Retina Tomograph (HRT), which is a confocal laser-scanning microscope. As a result, the depth value of the ONH obtained using the stereo retinal image pair was in accordance with that obtained using the HRT (r=0.91). These results indicate that the stereo fundus images could be useful for assessing the depth value of the ONH for the diagnosis of glaucoma.**

I. Introduction

The cup/disc (C/D) ratio, which is the ratio of the diameter of the depression (cup) to that of the optic nerve head (ONH, disc), is one of the important parameters for an early diagnosis of glaucoma. The C/D ratio is generally used in clinical practice because its value is greater in the case of glaucoma. The interpretation of the ONH, which actually has a 3-D structure, by using a 2-D image is subjective and there is a wide variation between the examination of the ONH by different observers and even between the examinations by the same observer [1]. A more quantitative alternative is to use the Heidelberg Retina Tomograph (HRT), which is a confocal laser-scanning microscope, for the acquisition and analysis of the 3-D measures of the ONH [2, 3]. It has been revealed that an HRT is capable of ONH imaging, and it is an established technique for detecting glaucomatous structural changes.

A computerized technique for the qualitative estimation of the depth of the ONH from the stereoscopic pairs of retinal-fundus images has been suggested for the 3-D analysis of the depression of the ONH [4, 5]. It has been shown that this technique is useful for the investigation of the 3-D measures of the ONH. However, the experimental results regarding the quantitative depth value calculated from the stereo image pair of the ONH have not been reported. Moreover, there have been no studies in which the depth value calculated from the stereo image pair has been compared with the HRT outputs.

In this study, an automatic method for reconstructing the 3-D structure of the ONH by using the stereo fundus images is proposed. In order to evaluate the accuracy of our method, the depth values of the ONH obtained from the stereo fundus image pairs are compared with the HRT measurement results.

Manuscript received April 2, 2007. This work was supported in part by a grant for the "Knowledge Cluster Creation Project" from the Ministry of Education, Culture, Sports, Science and Technology (MEXT), Japan.

T. Nakagawa, Y. Hayashi, A. Aoyama, T. Hara, H. Fujita and T. Yamamoto are with the Graduate School of Medicine, Gifu University, 1-1 Yanagido, Gifu 501-1194, Japan (e-mail: nakagawa@fjt.info.gifu-u.ac.jp).

Y. Hatanaka is with the Department of Electric Control Engineering, Gifu National College of Technology, 2236-2 Kamimakuwa, Motosu, Gifu 501-0495, Japan.

A. Fujita is with the Kowa Company, Ltd., 1-3-1 Shinmiyakoda, Hamamatsu, Shizuoka 431-2103, Japan.

M. Kakogawa is with the TAK Co., Ltd., 4-35-12 Kono, Ogaki, Gifu 503-0803, Japan.

II. Methodology

In our technique, the depth value is obtained from the stereo fundus image pair; it mainly consists of four processes. A stereo image pair consists of a "left image" and a "right image" captured from different perspectives. The stereo image pair can be generated by taking two shots with a parallel shift using a single-lens fundus camera or by taking a single shot using a stereo-fundus camera. In the first step, the images of the ONH region are cut out from the original fundus images in the first step. In the second step, the registration process of the stereo ONH image pair is performed in order to remove any displacements. In the third step, the "corresponding points" in each stereo ONH image are detected. In the fourth step, the depth values of the 3-D structures are calculated from the results of the disparities detected in the configuration of the corresponding points.

A. Cutout of the ONH region

The images of the ONH region were cut out from the original stereo image pair in order to reduce the processing area to expedite the subsequent steps. In this processing step, the fundus images were cropped to form quadrates at the position of the ONH region that was extracted automatically. The ONH region has relatively high pixel values in three channels (R, G, and B components) in the color stereo fundus image pairs. P-tile thresholding [6] can be applied to define a threshold for an approximate extraction of the ONH region because individual variations of the ONH do not vary significantly.

The blood vessels (BVs) running on the surface of the ONH interfered with the correct extraction of the ONH region

1-4244-0788-5/07/$20.00 ©2007 IEEE

in the P-tile thresholding operation. In order to solve this problem, the extraction of the ONH region was performed by using the images in which the BVs were erased. These erased pixels were then interpolated by using the RGB values of the pixels in the surrounding region. The pixel value P used in the interpolation was calculated as

$$P=\frac{\sum_{k=1}^{n}\frac{p_k}{l_k}}{\sum_{k=1}^{n}\frac{1}{l_k}}, \quad (1)$$

where p_k denotes the value of the pixels in the surrounding region, n is the number of surrounding pixels, and l_k is the distance between the interpolated pixel and each surrounding pixel.

The BVs were extracted by using the black-top-hat transformation, which is a type of grayscale morphological operation, from the G-component of the color fundus images. The structure element used in this transformation was a disc whose diameter was set to the same level as the thickness of the BVs in the ONH region. The regions containing BVs were extracted after applying the Otsu thresholding technique [7] to the black-top-hat-transformed image.

The center of the square of the cutout of the ONH region was the gravity point of the ONH region extracted from the images in which the BVs were erased. In this study, the size of the original fundus image was 1600 × 1200 pixels, the angle of view was 27°, and the size of the cutout region was 512 × 512 pixels, as shown in Fig. 1.

B. Registration of the stereo fundus image pair

The disparity, which is defined as the difference in the position of the corresponding points in the stereo image pair, depends on the change in the position of not only the camera but also the subject (subject's motion). The disparity due to the subject's motion affects the calculated result of the depth value. In order to accurately measure the depth value, it is necessary to rectify the disparity due to the subject's motion. However, it is difficult to determine the motion that induces the disparity only on the basis of observations.

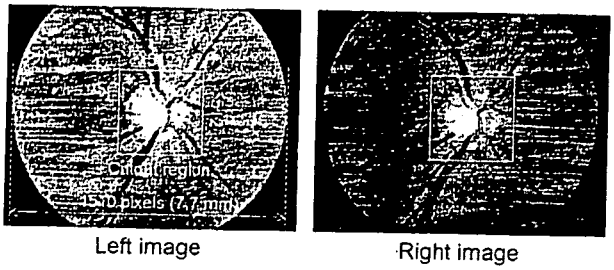

Fig. 1. Example of an original stereo fundus image pair and cutout region from the left and right images.

In the retinal fundus, the bell-shaped ONH has a dent on the opposite side, that is, the side facing the camera. Therefore, the cup region of the ONH exists at a distant position from the camera and the disparity is small. Theoretically, it is possible to use the pixels in the ONH region, which have small disparities, for image registration. However, the region of the retina around the ONH is more suitable for the image registration task because the blood vessels in the retina exist even on the curved surface; in this region, the right and left images exhibit a parallel shift. Moreover, the 3-D structure of the retinal region is simpler than that of the ONH. From the abovementioned description, the image registration for rectifying the disparity due to a subject's motion was performed by using the pixels from regions other than the ONH region.

In order to exclude the ONH region from the registration process, the pixels of a fundus image were allocated to two regions: the retina and the ONH region. The pixels in the retina region were used for registering the stereo image pair. The boundary between the two regions was obtained by automatically extracting the ONH region.

In the first step, a contour of the ONH region was extracted from two stereo fundus images. The ONH region has a tendency to have a higher pixel value than the other regions. Furthermore, the contour of the ONH region can be expressed with a smooth closed curve in many cases. Therefore, the contour that exhibits high edge intensity, which is defined as a change in the brightness, was extracted as the smooth closed curve by using an active-contour model [8].

In the next step, the registration of the stereo image pair was performed by using all the pixels of the images from regions other than the ONH region. If the positional error is minimum, the sum of all the differences between the pixel values of the two images will be minimum. Therefore, the right image was translated and rotated until the sum of all the differences was minimum. This registration procedure used the cross-correlation r between the two images, which is calculated as

$$r=\frac{\sum_{i=0}^{W}\sum_{j=0}^{H}\{L(i,j)-\bar{L}\}\{R(i,j)-\bar{R}\}}{\sqrt{\sum_{i=0}^{W}\sum_{j=0}^{H}\{L(i,y)-\bar{L}\}^2}\sqrt{\sum_{i=0}^{W}\sum_{j=0}^{H}\{R(i,j)-\bar{R}\}^2}}, \quad (2)$$

where L and R are the feature values in the coordinate system (i, j) of the left and right images, respectively; W and H, the width and height of the image, respectively; and $\bar{L}$ and $\bar{R}$, the average pixel values in the left and right images, respectively. The features used in the registration were the pixel values of the RGB components and its edge images created by the Sobel filter using the RGB values.

C. Disparity detection

The required disparity for obtaining the depth value was calculated from the location differences between the corresponding points. The detection of the corresponding points was performed using the pixels of the area within the registered ONH image pair. The detection of the corresponding points comprised the search for a point on the right image that corresponded to the reference point on the left image. The search was performed by setting up regions of interest (ROIs) including the pixels around the reference point and the candidate point separately. Two points on the left and right images having a similar texture in their respective ROIs were regarded as the corresponding points. The similarity was measured by the cross-correlation r defined as

$$r = \frac{\sum_{i=-W/2}^{W/2}\sum_{j=-H/2}^{H/2}\{L(x_L+i,y_L+j)-\bar{L}\}\{R(x_R+i,y_R+j)-\bar{R}\}}{\sqrt{\sum_{i=-W/2}^{W/2}\sum_{j=-H/2}^{H/2}\{L(x_L+i,y_L+j)-\bar{L}\}^2}\sqrt{\sum_{i=-W/2}^{W/2}\sum_{j=-H/2}^{H/2}\{R(x_R+i,y_R+j)-\bar{R}\}^2}}, \quad (3)$$

where L and R are the feature values of the pixels in the ROIs set in the ONH image pair, $\bar{L}$ and $\bar{R}$ are the average feature values of the ROIs, (x_L, y_L) is the coordinate of the reference point in the left image, (x_R, y_R) is the coordinate of the candidate point in the right image, and W and H are the width and height of the ROI, respectively.

The features used in the detection of the corresponding points were the pixel values of the RGB components and its edge images created by the Sobel filter using the RGB value. The parameters of this process are shown in Fig. 2. The size of the ROI was set to 21 × 21 pixels and the searching range was set to 41 × 23 pixels ([x_L – 5 pixels, x_L + 15 pixels]). The reference points arranged in the equally spaced positions and the interval were set to 4 pixels. The point having the maximum cross-correlation coefficient was considered to be the corresponding point. When the maximum value of the cross-correlation coefficient was smaller than a preset threshold value, it was assumed that the corresponding point of the reference point was not found. The disparity of the point that did not have a corresponding point was interpolated by the average of the disparities of the surrounding reference points.

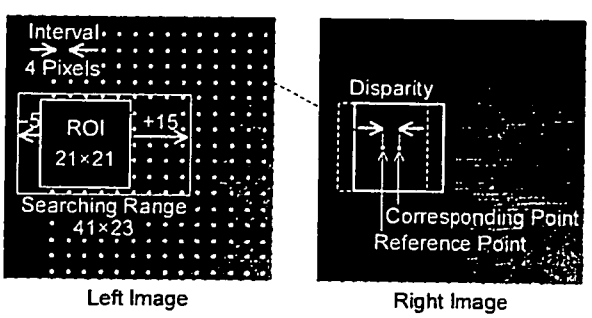

Fig. 2. Parameters in detecting the corresponding points in the left and right images.

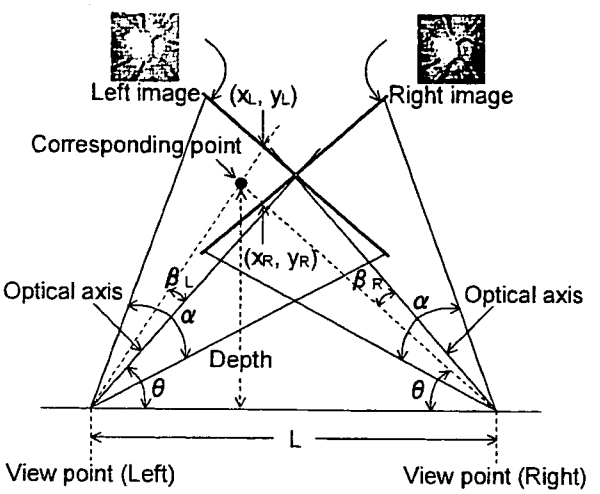

Fig. 3. Convergent visual system for depth calculation of stereo image pair.

D. Depth calculation

The depth value of the 3-D position was determined according to the value of the disparity in each location of the reference point. The depth value was calculated as

$$Depth = \frac{L \times \tan(\theta-\beta_L)\times\tan(\theta+\beta_R)}{\tan(\theta-\beta_L)+\tan(\theta+\beta_R)}, \quad (4)$$

$$\beta_L = \tan^{-1}\{x_L \times \tan(\frac{\alpha}{2}\times\frac{\pi}{180})\times\frac{2}{W}\}, \quad (5)$$

$$\beta_R = \tan^{-1}\{x_R \times \tan(\frac{\alpha}{2}\times\frac{\pi}{180})\times\frac{2}{W}\}, \quad (6)$$

and

$$x_R = x_L + disparity, \quad (7)$$

where x_L and x_R are the horizontal coordinates of the corresponding points in the left and right images, respectively. The original points in the coordinate system were arranged on the optical axis of the left and right viewpoints. α is the angle of view of the images; β, the angle between the position of the corresponding point and the optical axis; W, the width of the images; and L, the length of the baseline, which is the distance between the optical centers of the camera.

III. Results and Discussions

The proposed technique was evaluated using 12 normal fundus stereo image pairs. Figure 4 shows the depth values of the same ONH measured using the stereo image pairs and the HRT. The results of the depth measurements using the stereo image pairs agreed well with the results of the HRT at

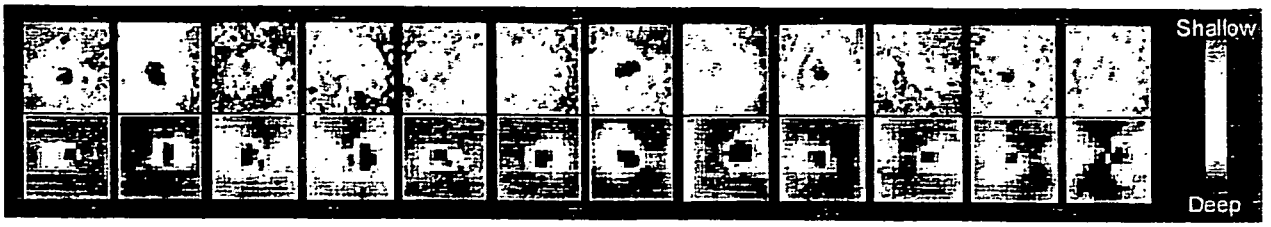

Fig. 4. The upper row shows the depth maps of the OHN from stereo fundus image pairs. The lower row shows the depth maps obtained using the HRT. The depth of the ONH obtained using the stereo images agreed with the results obtained using the HRT.

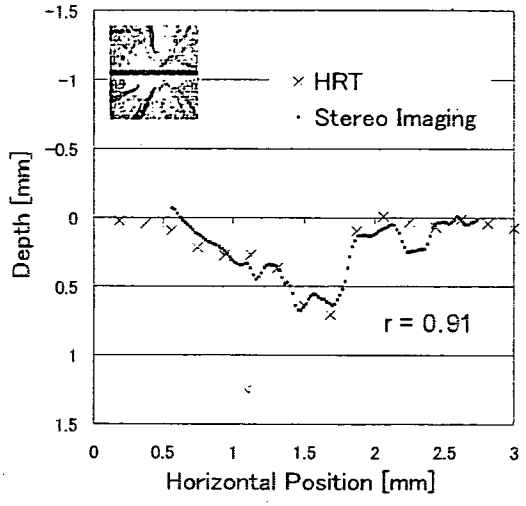

Fig. 5. Example of depth information obtained from the stereo fundus image pair and HRT.

corresponding levels. The depth values measured using the stereo image pairs fluctuated. This is due to the slight uncertainty in the disparity detection. It is presumed that the median filter can effectively eliminate this incorrect disparity. Figure 5 shows the profile trace along the center of the OHN. The correlation coefficient r between the two results obtained by the two methods was 0.91. This result indicates the validity of proposed method to obtain quantitative depth values.

IV. Conclusion

In this study, we conducted quantitative measurements of the depth value of an ONH region from the stereo fundus images. The depth values obtained from the stereo image pairs were in accordance with the results of the HRT. These depth values may be useful as assisting parameters for ophthalmologists in the diagnosis of the degree of glaucoma.

Acknowledgment

This work was partly supported by a grant for the Knowledge Cluster Creation Project from the Ministry of Education, Culture, Sports, Science and Technology, Japan. The authors would like to acknowledge the contribution of Dr. R. Shiraki of the Shiraki Eye Clinic for the acquisition of the HRT data.

References

[1] J. M. Tielsch, J. Katz, H. A. Quigley, A. Sommer, "Intraobserver and interobserver agreement in measurement of optic disc characteristics," Opthalmol., vol.95, no.3, pp.350–356, 1988.

[2] F. S. Mikelberg, C. M. Parfitt, N. V. Swindale, S. L. Graham, S. M. Drance, R. Gosine, "Ability of the Heidelberg Retina Tomograph to detect early glaucomatous visual field loss," J. Glaucoma, vol.4, no.4, pp.242–247, 1995.

[3] M. Iester, F. S. Mikelberg, S. M. Drance, "The effect of optic disc size on diagnostic precision with the Heidelberg Retina Tomograph," Ophthalmol., vol.104, no.3, pp.545–548, 1997.

[4] E. Corona, S. Mitra, M. Wilson, T. Krile, Y. H. Kwon, P. Soliz, "Digital stereo image analyzer for generating automated 3-D measures of optic disc deformatin in glaucoma, IEEE Trans. Med. Imaging, vol.21, no.10, pp.1244–1253, 2002.

[5] J. Xu, O. Chutatape, "Auto-adjusted 3-D optic disk viewing from low-resolution stereo fundus image," Computers in Biology and Medicine, vol.36, pp.921–940, 2006.

[6] J. R. Parker, "Algorithms for Image Processing and Computer Vision," Wiley Computer Publishing, 1997.

[7] N. Otsu, "A threshold selection method from gray-level histograms," IEEE Trans. Syst. Man. Cybern. vol.SMC-9, pp.62–66, 1979.

[8] M. Kass, A. Witikin, D. Terzopoulos, "Snakes: Active contour models," Int. J. Computer Vision, vol.1, pp.321–331, 1987.

Jpn J Ophthalmol 2007;51:379–389

DOI 10.1007/s10384-007-0468-8

CLINICAL INVESTIGATION

Decreased Nasal–Temporal Asymmetry of the Second-Order Kernel Response of Multifocal Electroretinograms in Eyes with Normal-Tension Glaucoma

Eijiro Asano[1], Kiyofumi Mochizuki[1], Akira Sawada[1], Ei-ichiro Nagasaka[2], Yuji Kondo[1], and Tetsuya Yamamoto[1]

[1]Department of Ophthalmology, Gifu University Graduate School of Medicine, Gifu, Japan; [2]Mayo Corporation, Inazawa, Japan

Abstract

Purpose: To determine whether multifocal electroretinograms (mfERGs) can provide an index for identification of glaucomatous optic neuropathy in patients with normal-tension glaucoma (NTG).

Methods: mfERGs were recorded in 30 normal volunteers (30 eyes) and 20 patients (20 eyes) with normal-tension glaucoma (NTG). Visual field examinations were performed with a Humphrey field analyzer, and all NTG patients had unilateral hemifield defects. The mfERGs were elicited by a binary m-sequence of flashes from 37 hexagonal elements that subtended an overall visual angle of 50° × 40°. The mfERGs were summed and analyzed for predetermined retinal loci. These mfERGs were compared with the perimetric findings of the corresponding visual fields.

Results: In normal volunteers, the amplitude of the second-order kernel within the central 5° of the nasal hemisphere was significantly smaller than in that of the temporal hemisphere (Wilcoxon signed-rank test, $P = 0.0001$). In NTG patients, this asymmetry of the two hemispheres was reduced or not present. The ratio of the amplitude of the mfERGs from the nasal and temporal hemispheres (N/T amplitude ratio) in normal control volunteers was significantly different from that of NTG patients with a hemifield defect (analysis of variance, $P = 0.0001$). When the cutoff value for the N/T amplitude ratio was set at 0.83 for discriminating glaucomatous eyes from normal eyes, the sensitivity was 65.0% with a specificity of 96.7%. The area under the receiver–operating characteristic curve of the N/T amplitude ratio was 0.86. The N/T amplitude ratio and the visual field indices were significantly correlated.

Conclusion: A decrease in the nasal–temporal asymmetry in the amplitude of the second-order kernel responses within the central 5° of glaucoma patients' eyes indicated a dysfunction of the inner retinal layers, including of the retinal ganglion cells. **Jpn J Ophthalmol** 2007;51:379–389 © Japanese Ophthalmological Society 2007

Key Words: hemifield visual field defects, multifocal electroretinogram, normal-tension glaucoma

Introduction

A number of electrophysiological tests have been used to determine whether the alterations of retinal function in glaucomatous eyes can be detected objectively. The main site of damage in eyes with glaucoma is most likely the lamina cribrosa,[1] and the damage eventually spreads retrogradely to the cell bodies of the retinal ganglion cells (RGCs). The dysfunction in glaucomatous eyes is in the RGCs and their axons. Therefore, standard flash electroretinograms (ERGs) do not provide critical information on early glaucomatous changes, because the cells generating conventional ERGs are located in the outer retina.[2] Thus, the functioning of the retina distal to the RGCs in glaucomatous optic neuropathy has been considered normal.[3,4]

Received: February 22, 2007 / Accepted: June 7, 2007
Correspondence and reprint requests to: Kiyofumi Mochizuki, Department of Ophthalmology, Gifu University Graduate School of Medicine, 1-1 Yanagido, Gifu-shi 501-1194, Japan
e-mail: mochi-gif@umin.ac.jp

Jpn J Ophthalmol
Vol 51: 379–389, 2007

The techniques for recording multifocal electroretinograms (mfERGs) have been refined, and the search for an objective method to detect the pathological changes in glaucomatous eyes has continued with mfERGs. Thus, Bearse et al.[5] suggested that the second-order kernels of mfERGs might have a component that indicates a decrease in surviving RGCs throughout the retina in glaucomatous eyes. Sutter and Bearse[6,7] extracted an optic nerve head component (ONHC) from the second-order kernel of mfERGs, and suggested that this ONHC was a signal originating from RGCs and was altered in eyes with glaucomatous optic neuropathy. In addition, they reported that the spatial distribution of the amplitudes of the ONHC in normal subjects was steeper than that of the other retinal components, with a peak in the center of the visual field.[6] From these findings, we assumed that the mfERGs elicited from the central retina receive a larger contribution from the ONHC than more peripheral mfERGs.

Studies on glaucomatous eyes using mfERGs have been performed with flicker stimulation,[8–10] global flash stimuli,[11] s-wave stimulation,[12] and low-contrast stimuli.[8,13,14] In these studies, no significant differences were found in the amplitudes of mfERGs between glaucoma and control subjects,[9] and only a slight prolongation of latencies was found in eyes with glaucoma.[8,10,11] Moreover, they found no significant correlation between the amplitudes of the mfERGs and visual field parameters. One of the reasons for the lack of differences might be that the slight alterations of the ONHC were buried in the larger retinal components when the responses were grouped in relatively large quadrants or rings over the entire stimulus field.

Several studies on normal eyes have shown that the amplitudes of mfERGs in the nasal hemifield are significantly different from those in the temporal hemifield, that is, there is a nasal–temporal (N/T) asymmetry.[5,6,13–16] We hypothesized that this asymmetry was related to local differences in the distribution of the ONHC, and, thus, this asymmetry should be altered by dysfunction of the RGCs in glaucomatous eyes. Our analyses focused on the changes of mfERGs around the central region, because we believe that the small difference in the ONHC between normal and glaucomatous eyes should be detected more clearly in this region. We also analyzed the ratio of the amplitudes of the mfERGs from the nasal and temporal hemispheres and between the superior and inferior hemispheres to search for any alterations in asymmetry in the mfERGs.

Subjects and Methods

Control and Normal-Tension Glaucoma Subjects

Data were obtained from 30 control volunteers (30 eyes) and 20 patients (20 eyes) with normal-tension glaucoma (NTG). The criteria used to select the control subjects were normal findings on all ocular examinations, best-corrected visual acuity of 20/30 or better, normal visual fields, and no history of ocular or neurological diseases.

Although glaucoma is characterized by a unique pattern of visual field defects that correspond to the optic nerve head excavation, the extent of glaucomatous visual field defects is highly variable among patients. We selected NTG patients with visual field defects confined to one hemifield, because mfERG abnormalities would be more easily detected in the summed mfERGs in this type of patient. Patients were diagnosed with NTG when they were found to have the following: visual field loss distinctive to glaucoma, cupping of the optic nerve head, and intraocular pressure of <20 mmHg, including 24-h diurnal values. In addition, all of the NTG patients had visual field abnormalities of 5 dB or greater at two or more adjacent points, or abnormalities of 10 dB or greater at one or more points, below the age-adjusted average control value according to a Statpac single-field analysis. Although the glaucoma subjects could have some normal findings during ocular examinations, they all had glaucomatous optic neuropathy, no history of any medications that could affect pupil diameter, no history of any ocular surgery, and a best-corrected visual acuity of 20/30 or better.

Written informed consent was obtained from all participants, and all procedures were performed in compliance with the tenets of the Declaration of Helsinki. The experimental protocols were approved by the Institutional Board of Research Associates of Gifu University Graduate School of Medicine.

Visual Field Testing

All visual field examinations were performed with a Humphrey field analyzer (Zeiss-Humphrey, San Leandro, CA, USA) using the central 30-2 static threshold program. Results that met the reliability criteria for false-negative responses of <30%, false-positive responses of <15%, and fixation loss rates of <15% were used for the analyses.

The glaucoma patients were divided into two groups according to their visual field defects; those with defects in the superior hemifield were placed in one group, and those with defects in the inferior hemifield in a second group. The presence of a unilateral hemifield defect was defined on the basis of the total deviation probability plot as a hemifield with eight or more test points with $P < 5\%$, either in a cluster or sporadically dispersed. In contrast, an intact hemifield was defined as one with no points worse than the 2% probability level, and no more than two points at the 2%–5% probability level.[17]

Multifocal ERG Techniques

A Visual Evoked Response Imaging System Science 4 (Electro-Diagnostic Imaging, EDI, Redwood City, CA, USA) was used to record the mfERGs. The eye used for the recordings was optically corrected, and the pupil was dilated to at least 8 mm in diameter with topical 0.5% tropicamide and 0.5% phenylephrine (Mydrin-P; Santen Phar-

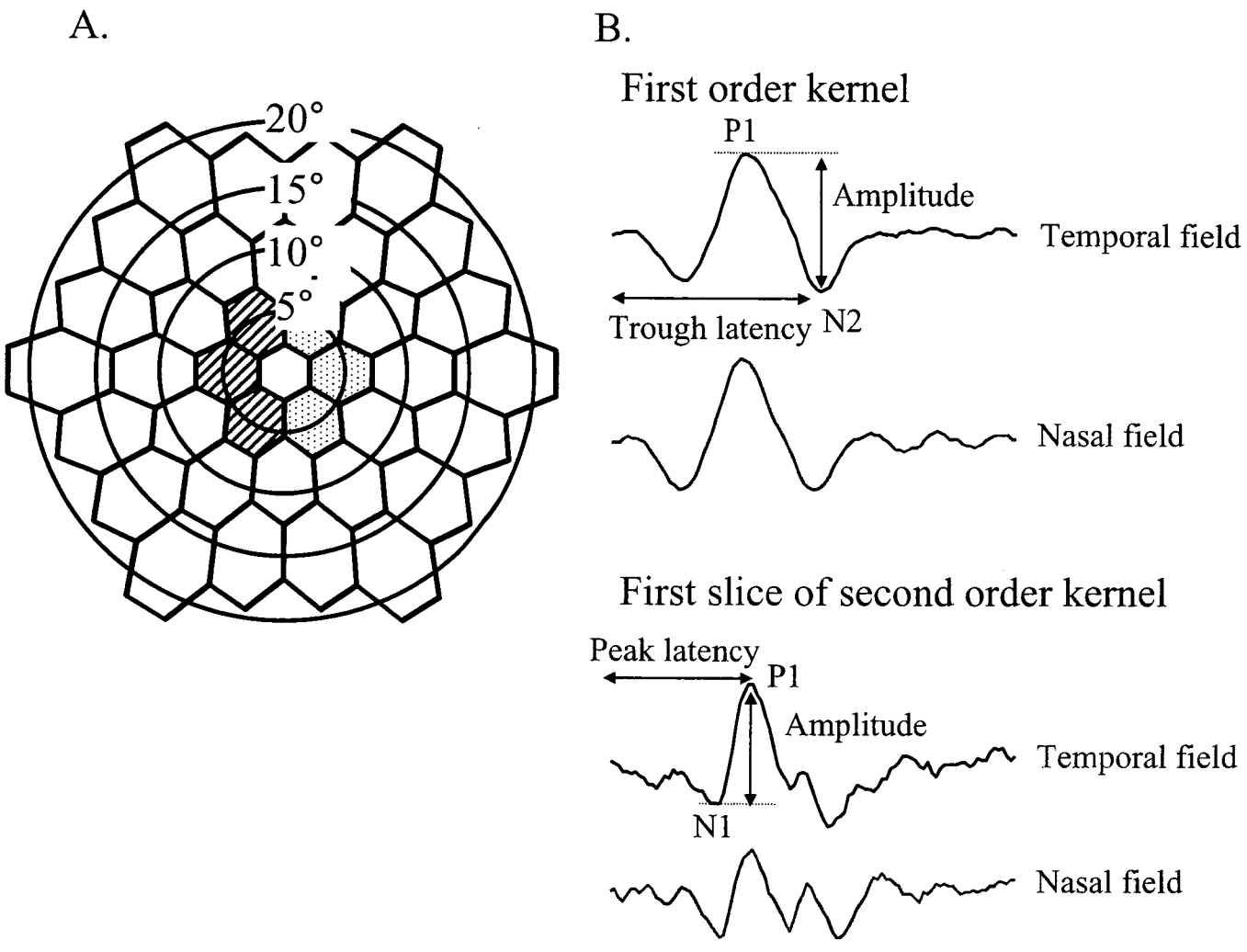

Figure 1A, B. Pattern of the 37-hexagon stimulus array with circles indicating radii of 5°, 10°, 15°, and 20°. **A** Waveforms and measurements of the first-order kernel response (*upper right*), and the first slice of the second-order kernel response (*lower right*) obtained from multifocal electroretinograms (**B**).

maceutical, Osaka, Japan). A bipolar contact lens electrode (Mayo, Inazawa, Japan) was placed on the cornea, which was anesthetized with topical oxybuprocaine hydrochloride (Benoxil). The contralateral eye was covered. Hydroxyethylcellulose gel (Scopisol) was used to keep the cornea moist and to form a good electrical contact between the contact lens electrodes and the cornea. A gold-cup electrode was attached to the right earlobe and served as the ground.

The visual stimulus consisted of 37 hexagons that were displayed on a monochrome computer monitor (QB1781; Chuomusen, Tokyo, Japan). The overall area subtended by the stimulus pattern was 50° by 40° (Fig. 1A). Each element was independently alternated between black (5 cd/m^2) and white (200 cd/m^2) at a frame rate of 75 Hz according to a binary m-sequence. The contrast of the hexagons was 95.1%. The mfERGs were recorded with bandpass filters of 10 to 300 Hz, and the total recording time was approximately 8 min. Recordings with eye movements or blinks causing artifacts were discarded and recorded again. An artifact elimination technique was applied once; however, spatial smoothing was not used.

Response Analyses

The first negative trough (N1), the first positive peak (P1), and the second negative trough (N2) were studied. The amplitude from P1 to N2 of the first-order kernel response, and that from N1 to P1 of the first slice of the second-order kernel response, were used in the analyses. In addition, the latencies of N2 of the first-order kernel and P1 of the second-order kernel (Fig. 1B) were measured.

For the analyses, the mfERGs were initially grouped into three concentric rings; central, middle, and peripheral rings (Figs. 2A and B). Then, the mfERGs from the superior field in each ring were summed and compared with the summed mfERGs in the inferior ring. Similarly, the summed mfERGs from each ring in the nasal hemisphere were compared with

Jpn J Ophthalmol
Vol 51: 379–389, 2007

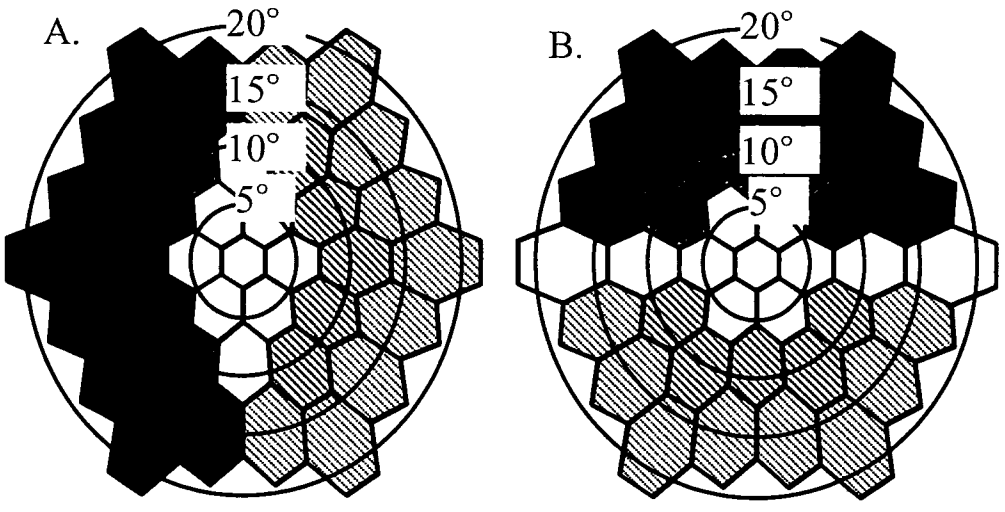

Figure 2A, B. Pattern of hexagons grouped in concentric rings with similar eccentricities (marked by different shadings). For further analysis, hexagons were separated and averaged according to hemisphere: temporal and nasal hemispheres (**A**), or superior and inferior hemispheres (**B**). Hexagons lying on the horizontal or vertical midline through the macula were not used in the analysis.

Table 1. Demographic data of normal volunteers and NTG patients

	Normal volunteers (30 eyes of 30 subjects)	NTG patients (20 eyes of 20 subjects)	*P* value*
Sex (male/female)	10/20	11/9	0.1283
Right/left	15/15	8/12	0.3541
Age (years)	57.6 ± 10.0 (43–75)	59.7 ± 8.9 (40–73)	0.4399
Refractive error (D)	−0.33 ± 2.10 (−4.75 to +2.75)	−2.51 ± 2.94 (−8.75 to +2.25)	0.0084

Values are means ± SD (range).
NTG, normal-tension glaucoma.
*Mann-Whitney *U* test or Fisher's direct probability test.

the corresponding averaged mfERGs in the temporal hemisphere.

The ratios of the amplitudes of the mfERGs of the nasal to the temporal hemisphere (N/T), and of the superior to the inferior hemisphere (S/I) were calculated to evaluate the asymmetry. For all eyes, the amplitudes, implicit times, and N/T amplitude ratios of the summed responses in the nasal hemifield were compared with the responses in the temporal hemifield. Similarly, the summed responses in the superior hemifield were compared with the summed responses in the inferior hemifield.

To compare the mfERGs with the thresholds measured by Humphrey perimetry of the corresponding visual field, the thresholds in NTG subjects were separately averaged according to distance from the macula, that is, within the central 5°, 10°, 20°, and 30°. We examined the relationships between point thresholds or total deviation obtained from the corresponding visual field area and the N/T amplitude ratio of the first-order kernel response within the central 5°, and of the second-order kernel response within the central 5°.

Statistical Analyses

The Wilcoxon signed-rank test, Mann-Whitney *U* test, and Fisher's direct probability test were used. In addition, one-way analysis of variance (ANOVA) and Scheffé post hoc comparisons were used to determine the statistical significance of the differences in the amplitudes and implicit times in the first- and second-order kernels of the mfERGs among the three groups. Spearman rank correlations were used to assess relationships between point thresholds or total deviation and the N/T amplitude ratio of the first-order kernel and that of the second-order kernel. A *P* value of <0.05 was considered significant.

Results

The demographic data of the control subjects and NTG patients are presented in Tables 1 and 2. The mean age of the normal volunteers was 57.6 ± 10 years (range, 43–75 years), and that of NTG patients was 59.7 ± 8.9 years (range, 40–73 years). The mean refractive error of the NTG patients (−2.51 D) was significantly higher than that of the normal volunteers (−0.33 D; $P = 0.0084$). Of the 20 NTG patients, ten had visual field defects predominantly in the superior hemifield, and ten in the inferior hemifield.

Comparison of First-Order and Second-Order Kernels between Controls and NTG Patients

Representative waveforms of the first-order and second-order kernels of the mfERGs recorded from a normal vol-

Table 2. Demographic data for NTG patients with hemifield visual field defects

	Superior hemifield defect-dominant group (10 eyes of 10 patients)	Inferior hemifield defect-dominant group (10 eyes of 10 patients)	*P* value*
Sex (male/female)	5/5	6/4	>0.9999
Right/left	3/7	5/5	0.6499
Age (years)	61.9 ± 5.20 (60–68)	57.4 ± 11.75 (40–73)	0.6766
Refractive error (D)	−1.28 ± 2.91 (−8.75 to +0.50)	−3.75 ± 2.71 (−6.25 to +2.25)	0.0343
HFA central 30-2			
MD (dB)	−6.67 ± 2.99 (−12.62 to −3.55)	−7.97 ± 4.78 (−15.43 to −1.33)	0.5453
PSD (dB)	12.26 ± 1.66 (9.35–13.84)	11.73 ± 4.30 (6.40–18.36)	0.5453
CPSD (dB)	11.93 ± 1.63 (9.21–13.62)	11.49 ± 4.27 (6.22–18.30)	0.6500

Values are means ± SD (range).
HFA, Humphrey field analyzer; MD, mean deviation; PSD, pattern standard deviation; CPSD, corrected pattern standard deviation.
*Mann-Whitney *U* test or Fisher's direct probability test.

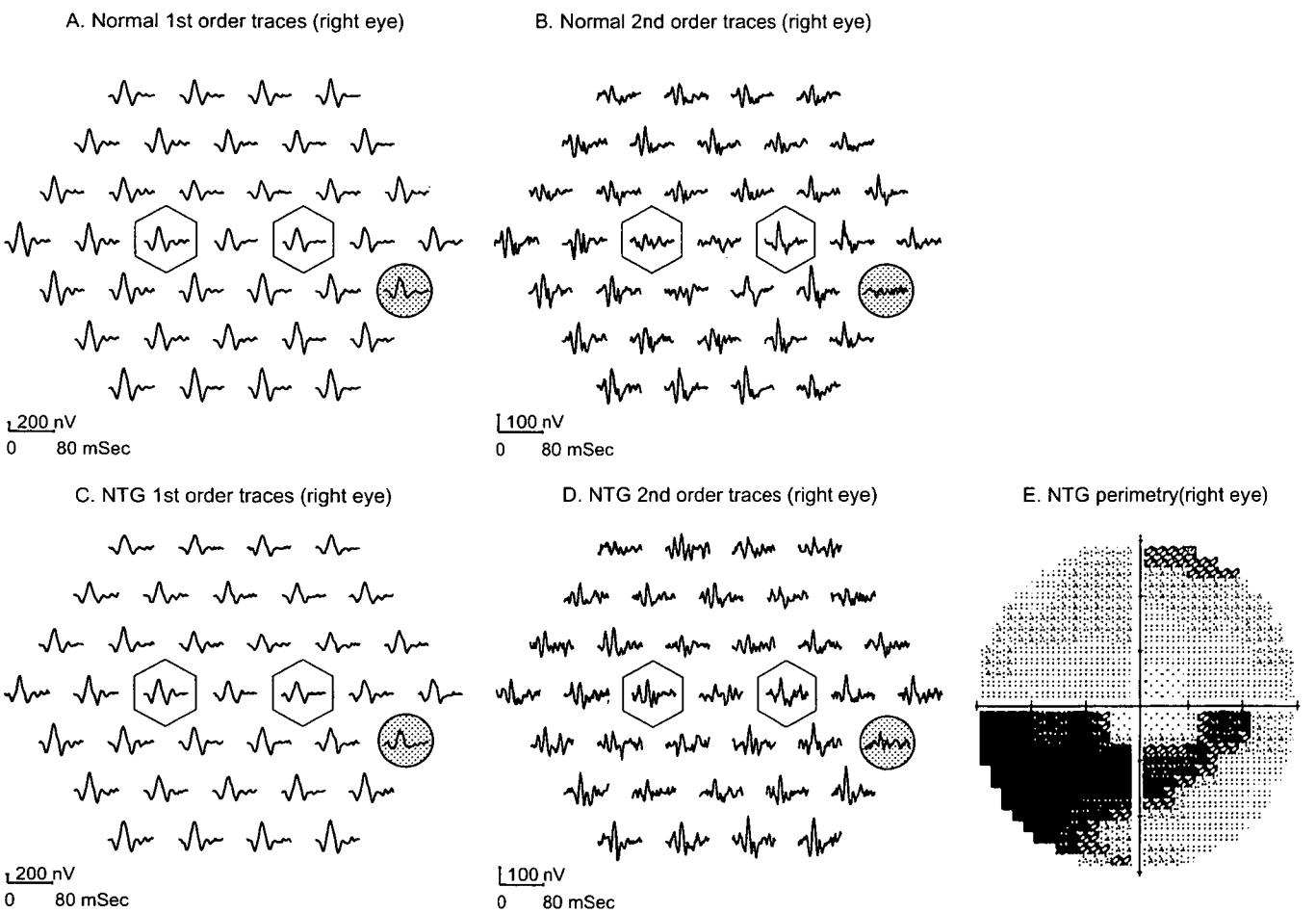

Figure 3. Representative waveforms of the first-order kernel and the first slice of the second-order kernel obtained from a normal volunteer (*upper*) and a normal-tension glaucoma (*NTG*) patient (*lower*).

unteer and a NTG patient are shown in Fig. 3. The amplitude of the second-order kernel for the nasal 5° central hexagon in the normal volunteers was significantly smaller than that of the temporal hemisphere (Fig. 3B, open hexagons). This asymmetry was less or was not present in the NTG patients (Fig. 3D).

Summed Responses from Concentric Rings in Normal Volunteers

In normal volunteers, the amplitudes of the first-order kernel in the temporal and superior hemisphere of all three rings were significantly smaller than those in the corre-

Jpn J Ophthalmol
Vol 51: 379–389, 2007

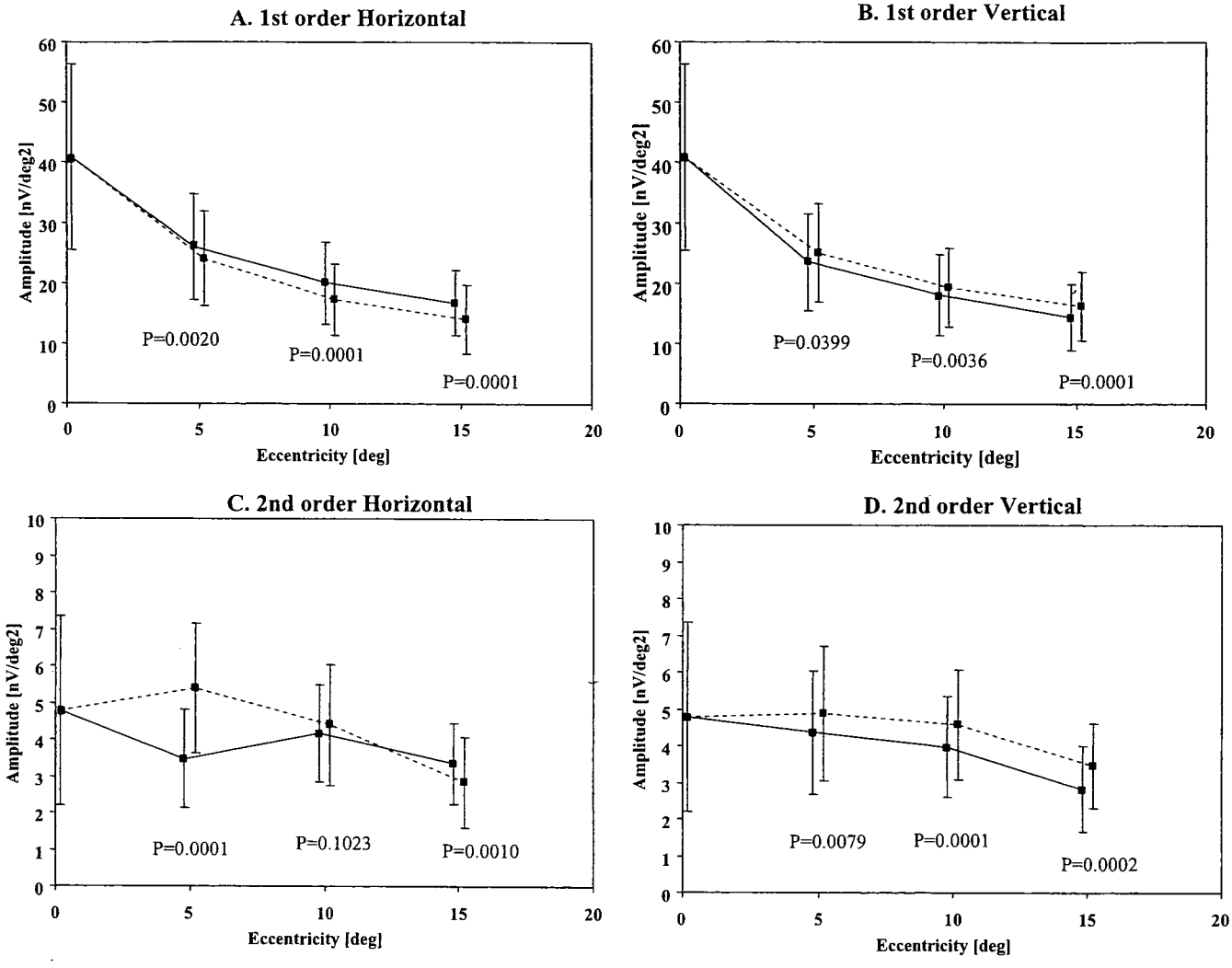

Figure 4A–D. Mean amplitudes of the first-order kernel horizontally from the center to the temporal or nasal retinal region (**A**), and along a vertical line from the center to the superior or inferior retinal region (**B**) in the normal control group. Mean amplitudes of the second-order kernel horizontally from the center to the temporal or nasal retinal region (**C**), and along a vertical line from the center to the superior or inferior retinal region (**D**) in the normal control group. **A, C** *Solid lines*, nasal field; *broken lines*, temporal field. **B, D** *Solid lines*, superior field; *broken lines*, inferior field.

sponding nasal and inferior hemispheres, respectively (Fig. 4; Table 3). The trough latencies of the mfERGs in the temporal hemisphere of all three rings were significantly longer than the corresponding nasal ones (Fig. 5; Table 3). In addition, the trough latency in the superior hemisphere within the central 5° was significantly longer than that of the responses in the inferior hemisphere (Fig. 5; Table 3).

The amplitude of the second-order kernel of the mfERGs in the superior hemisphere was significantly smaller than that in the inferior hemisphere (Fig. 4; Table 4). However, unlike with the first-order kernel, the amplitude of the mfERGs in the central 5° and 10°, but not that of the central 15°, in the nasal hemisphere were smaller than those in the temporal hemisphere (P = 0.0001 and 0.1023, respectively, Wilcoxon signed-rank test; Table 4).

The peak latencies of the responses from the superior and inferior hemifields and between the nasal and temporal hemifields in the central 5° were significantly different for the three different rings (Fig. 5; Table 4).

Summed Responses from Concentric Rings in NTG Patients

In general, the pattern of the first-order kernels in NTG patients was similar to that of normal subjects. For all three eccentricities, the amplitudes of the first-order kernel in the temporal and superior hemisphere were smaller than those in the nasal and inferior hemispheres (Table 3). The trough latency in the temporal hemisphere was more prolonged than that in the nasal hemisphere (Table 3). However, there was a difference in the trough latency for the central 10° and 15° between the superior and inferior hemispheres in the superior hemifield-dominant glaucoma group.

Table 3. Parameters of the mfERG first-order kernel response within the central 5° in glaucoma patients compared with that in normal volunteers

	Normal	Superior-dominant	Inferior-dominant	*P* value*			ANOVA *P* value
				Normal	Superior	Inferior	
Amplitude [nV/deg2]							
Nasal hemifield	26.1 ± 8.74	24.6 ± 8.85	22.6 ± 6.52	0.0020	0.0770	0.0069	0.5326
Temporal hemifield	24.1 ± 7.91	22.2 ± 7.66	20.2 ± 6.45				0.3695
Superior hemifield	23.5 ± 8.08	21.2 ± 6.63	19.3 ± 5.25	0.0399	0.1141	0.0068	0.2776
Inferior hemifield	25.0 ± 8.17	23.9 ± 9.82	21.6 ± 6.78				0.5465
Nasal/temporal hemifield	1.08 ± 0.11	1.11 ± 0.09	1.13 ± 0.11				0.4856
Superior/inferior hemifield	0.95 ± 0.13	0.92 ± 0.12	0.91 ± 0.07				0.6127
Trough latency [ms]							
Nasal hemifield	42.5 ± 1.31	42.8 ± 1.60	42.6 ± 1.27	0.0133	0.2864	0.0642	0.8429
Temporal hemifield	42.9 ± 1.30	43.1 ± 1.33	43.1 ± 1.10				0.8695
Superior hemifield	42.5 ± 1.31	43.1 ± 1.75	42.6 ± 1.29	0.0028	0.5750	0.6741	0.5835
Inferior hemifield	43.1 ± 1.31	43.3 ± 1.11	42.9 ± 0.92				0.7457

Values are expressed as mean ± SD.
mfERG, multifocal electroretinogram; ANOVA, analysis of variance.
*Wilcoxon signed-rank test: nasal versus temporal hemifield or superior versus inferior.

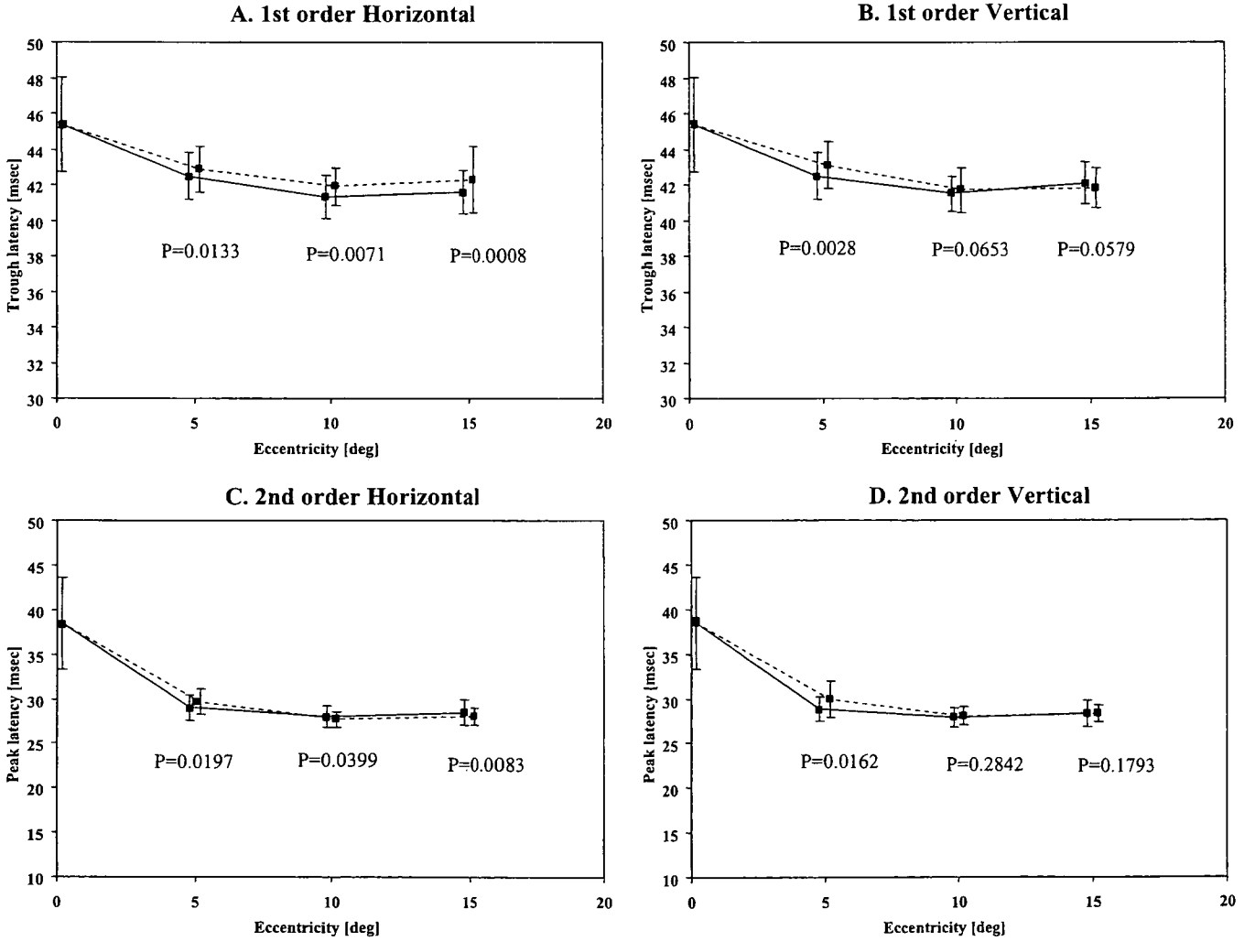

Figure 5A–D. Mean trough latency of the first-order kernel horizontally from the center to the temporal or nasal retinal region (**A**), and vertically from the center to the superior or inferior retinal region (**B**) in the normal control group. Mean peak latency of the second-order kernel response horizontally from the center to the temporal or nasal retinal region (**C**), and vertically from the center to the superior or inferior retinal region (**D**) in normal control groups. **A, C** *Solid lines*, nasal field; *broken lines*, temporal field. **B, D** *Solid lines*, superior field; *broken lines*, inferior field.